lubricants

MDPI

Article

Vibration Prediction and Optimization of Aeronautical Angular Contact Ball Bearings Considering Surface Waviness

Beiqi Sun [1], Dongfeng Wang [2,4,*], Yongxiang Su [2], Ning Jin [4], Yanjun Guo [5] and Lai Hu [3,6,*]

[1] School of Mechanical and Electrical, Luoyang Polytechnic, Luoyang 471003, China
[2] School of Mechanical Engineering, Tianjin University, Tianjin 300072, China
[3] Hefei Bolin Advanced Materials Co., Ltd., Hefei 230000, China
[4] Luoyang Bearing Science and Technology Co., Ltd., Luoyang 471003, China
[5] China Academy of Machinery Science and Technology Group Co., Ltd., Beijing 100044, China
[6] State Key Laboratory of Tribology in Advanced Equipment, Tsinghua University, Beijing 100084, China
* Correspondence: scholar_06@163.com (D.W.); laifinial@163.com (L.H.)

Abstract

Surface waviness is one of the most important factors affecting bearing vibration. How to effectively control waviness in actual production is a technical challenge in bearing mass production at present. This study established a ball bearing vibration analysis model based on the relationship between raceway waviness and bearing vibration, analyzed the contact between bearing balls and raceway waviness, studied the influence of waviness amplitude A, order nv, ball diameter Dw and rotational speed v on rolling bearing vibration, and given a bearing vibration prediction method and optimization control model based on waviness amplitude and order. Taking the angular contact ball bearing 7008/P4 as an example, experimental verification was carried out with different waviness states in four processes: coarse grinding, fine grinding, ultra-precision and polishing. The error between the model calculation results and the actual test results does not exceed 5%, which had good accuracy and practicality. The results shown that the amplitude of waviness had the greatest influence on vibration, followed by the order of waviness, and the influence was more significant with the increase of rotational speed.

Keywords: surface waviness; precision ball bearings; vibration; machining accuracy

1. Introduction

As an extremely important key basic component, rolling bearings are widely used in important fields such as aerospace, large wind power equipment, weapons and equipment, high-speed railways and buses, automobile industry, industrial equipment, and precision machine tools, with a global annual output value of approximately US$50 billion [1–4]. Its operating state has a significant impact on the accuracy, reliability and lifespan of the entire mechanical system [5–8]. Surface waviness is an important index to reflect the microscopic geometry error of part surface. As a key component of mechanical equipment, rolling bearings directly affect the working performance of the entire mechanical system [9,10]. Although the processing technology and accuracy of bearings have been greatly improved, the influence of factors such as machine tool accuracy, fixture positioning error and vibration inevitably leads to shape errors such as waviness on the raceway surface of bearings [11,12]. Therefore, the study of bearing vibration characteristics based on bearing waviness models under actual working conditions is of great significance [13].

Check for updates

Received: 9 October 2026
Revised: 6 November 2026
Accepted: 10 November 2026
Published: 12 November 2026

Copyright: © 2026 by the authors. Licensee MDPI, Basel, Switzerland. This article is an open access article distributed under the terms and conditions of the Creative Commons Attribution (CC BY) license.

Fan et al. [14] investigated the relationship between the waviness observed on the surfaces of bearing raceways and rollers and electrical erosion corrosion. Lou et al. [15] revealed the microscopic characteristics and formation mechanism of bearing waviness damage to the entire machine. Studies have shown that waviness with alternating "bright" and "dark" shapes are produced on GCr15 bearing housings. Garnham et al. [16] studied the relationship between waviness and vibration coefficient of rolling bearings in dry wear tests. Pan et al. [17] established a dynamic model that considers the waviness parameters of the inner and outer rings for the vibration characteristics caused by bearing waviness and local defects and proposed a time-varying displacement excitation local defect model based on piecewise functions. The results show that the proposed model can effectively identify waviness characteristic frequencies (such as ball passage frequency and its harmonics) and local defect impact signals. Harder et al. [18] studied the relationship between the performance of thrust ball bearings under continuous mechanical loads at multiple stages and the degree of waviness. The critical points of gray matte and corrugated surfaces are defined. Song et al. [19] studied the basic manifestations of electrical bearing damage, especially the formation of waviness on the bearing raceway surface and the transformation process of martensite to ferrite. When the current density exceeds 0.95 A/mm^2, the wear morphology of the bearing can be observed on the study surface. Zhou et al. [20] analyzed the evolution of contact load and corrugated surface stress during wear failure of cylindrical roller bearings. The results show that the contact stress in the inner raceway is greater than the contact stress in the outer raceway, and the contact stress in both the inner raceway and the outer raceway increases with the increase of the bearing wear level, with the increase in the inner raceway being greater than the increase in the outer raceway. Graf et al. [21] studied the results of durability tests of thrust bearings. Changes in surface waviness were analyzed using the Abbott–Firestone curve. These findings indicate that testing with additional electrical loads resulted in a significant reduction in roughness peaks. Correlation with acceleration measurements is performed. Furthermore, it is indicated that electrical loads may have an effect on light load stiffness. Tauviqirrahman et al. [22] proposed a new concept of the change in waviness on the raceway surface of a bearing after applying a load. The aim is to reduce bearing noise and improve load support without affecting friction. Simulation calculations show that the proposed improved bearing can significantly reduce bearing noise, enhance bearing capacity, and reduce friction. Narwat et al. [23] investigated the effects of bearing surface waviness orientation, turbulence (Reynolds number), and fluid flow coefficient on bearing film pressure, minimum film thickness, frictional torque, and stiffness coefficient. The results indicate that the waviness on the bearing surface tends to provide high film thickness values, but also enhances frictional torque. Litwin [24] studied that the surface waviness of the journal and bushing has an important impact on the performance of bearings. The results show that the waviness height has a great influence on the movement resistance and working performance of bearings. Yunlong et al. [25] established a dynamic model of angular contact ball bearings to study the influence of raceway surface waviness on ball movement and subsurface stress, in which the friction coefficient between the balls and the raceway is evaluated by an engineering method that considers surface waviness and slip-induced temperature rise.

Li et al. [26] studied wheel wear and rolling contact fatigue of subway vehicles under corrugation. Through statistical analysis of field data, the characteristics of ripples under service conditions are determined, and the ripples are applied to the established vehicle-rail coupling dynamics model. Then, the wear index and friction work were studied as wheel wear indexes. The results shown that the increase of surface fatigue index and cumulative fatigue in the wavelength range of 30–90 mm was 1.52 times and 6.16 times that in the wavelength range of 90–210 mm, respectively. Liu et al. [27] studied the friction and wear

performance of bearing roller raceway surfaces under different textures in order to improve tribological performance and service life. The results show that the bearing capacity of oil film is obviously improved under cavitation conditions. An increased textured area fraction reduces the coefficient of friction and improves the wear resistance of the contact pair, while an increased texture orientation angle leads to a deterioration in lubrication performance. Yue et al. [28] investigated the friction and wear characteristics of lubricants used in steel and ceramic bearings. The frictional behavior of aerospace lubricants was evaluated in four material pairs over a temperature range from ambient temperature to 170 °C. Meanwhile, the friction characteristics of waviness were studied. The results show that aerospace lubricants exhibit excellent tribological properties in Si3N4-based systems compared to steel/steel systems, characterized by lower friction coefficients and less wear. Hu et al. [29–32] conducted a comprehensive study on the waviness, vibration and wear characteristics of bearings. The bearing characteristics were comprehensively analyzed through design, manufacturing and service experiments. The results show that the wear of the inner ring is greater than that of the outer ring, and the corrugated surface layer belongs to the nanocrystalline layer, which is about 400 nm. Yin et al. [33,34] used fault diagnosis methods to identify bearing lifespan. At the same time, the algorithm and experimental verification were carried out according to the basic error parameters of bearings (roughness and corrugation), and the basic characteristic signals of bearing life were obtained. In addition, many scholars have conducted detailed research on surface waviness, surface properties, simulation methods [35,36] and surface microscopic changes [37–39].

Most of the above references have studied the influence of corrugation on bearing vibration. However, for actual working conditions, ripple degree is a non-directly observable parameter. For example, reference [14] clearly states that the ripple degree is related to electrical erosion corrosion, but it cannot be directly observed in time work. For example, in references [16,21], the authors used corrugation and bearing vibration models to explore the influence between them, and also analyzed the changes in bearing corrugation observed through durability experimental data. But that is just a brief discussion. In order to deeply study the relationship between bearing corrugation and vibration influence, this paper deeply analyzes and constructs the relationship between channel corrugation and bearing vibration and establishes a theoretical model of ball bearing vibration. Meanwhile, based on the contact between bearing balls and raceway corrugations, the influence of the amplitude, order, ball diameter and rotational speed of bearing raceway corrugations on rolling bearing vibration is studied. Through the establishment of bearing vibration prediction method and optimization control model for corrugation amplitude and order, the accuracy of the model is verified by simulation and experiment. This model has high accuracy when studying angular contact ball bearings, and its main range is similar to that of bearings of size 7008. During the experiment, the high-end bearing 7008 was used as the carrier to conduct experiments and verifications on different corrugation states from the processing technology and procedures (four procedures: coarse grinding, fine grinding, ultra-precision, and polishing). The influence factors between bearing manufacturing performance and experimental scheme on bearing vibration and ripple degree are repeatedly explained. This is also the main academic contribution and innovation of this study.

2. Theoretical Model Analysis

2.1. Mathematical Model of Surface Waviness

The shape of the surface waviness of the rolling bearing raceway can be assumed to be a sinusoidal waveform, and the wavelength of the waviness is assumed to be much larger than the size of the Hertz contact area between the rolling body and the raceway [40–42]. Here, only a single sinusoidal signal is used to simulate and analyze the influence of

surface waviness on contact vibration, assuming that surface roughness is described by Equation (1).

$$\begin{cases} x(t) = Rwt \\ y(t) = A\sin(n_v x) \end{cases} \tag{1}$$

where t is time, s. w is the rotational angular velocity of the bearing, rad/s. n is the order of the surface waviness, $x_{(t)}$ is the axial coordinate of a point on the corrugated surface, R is the radius, $y_{(t)}$ is the longitudinal coordinate of a certain point on the waviness surface, which is the waviness value of the ferrule surface, and A is the amplitude of the ripple. Figure 1 is a corrugated surface topography of Equation (1).

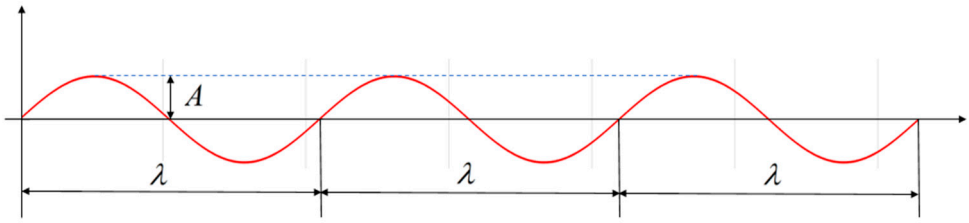


Figure 1. Schematic diagram of bearing groove surface waviness.

2.2. Ripple Excitation Model

During bearing movement, the longitudinal vibration caused by the waviness degree has its vibration displacement, vibration velocity, and acceleration set to y_s, y_v, and y_a, respectively. Vibration displacement is the change in the displacement of the spherical center in the Y-axis direction. Vibration velocity and acceleration can be obtained by calculating the first and second derivatives of $Y_{(t)}$ respectively according to the general curve Equation (2) of the spherical center trajectory to obtain Equation (3).

$$\begin{cases} X(t) = x(t) - \frac{Ry'(t)}{\sqrt{x'(t)^2+y'(t)^2}} \\ Y(t) = y(t) + \frac{Rx'(t)}{\sqrt{x'(t)^2+y'(t)^2}} \end{cases} \tag{2}$$

$$\begin{cases} Y(t) = y_s \\ Y'(t) = y_v \\ Y''(t) = y_a \end{cases} \tag{3}$$

The vibration displacement is shown in Equation (2).

The vibration acceleration formula is expanded to Equation (4).

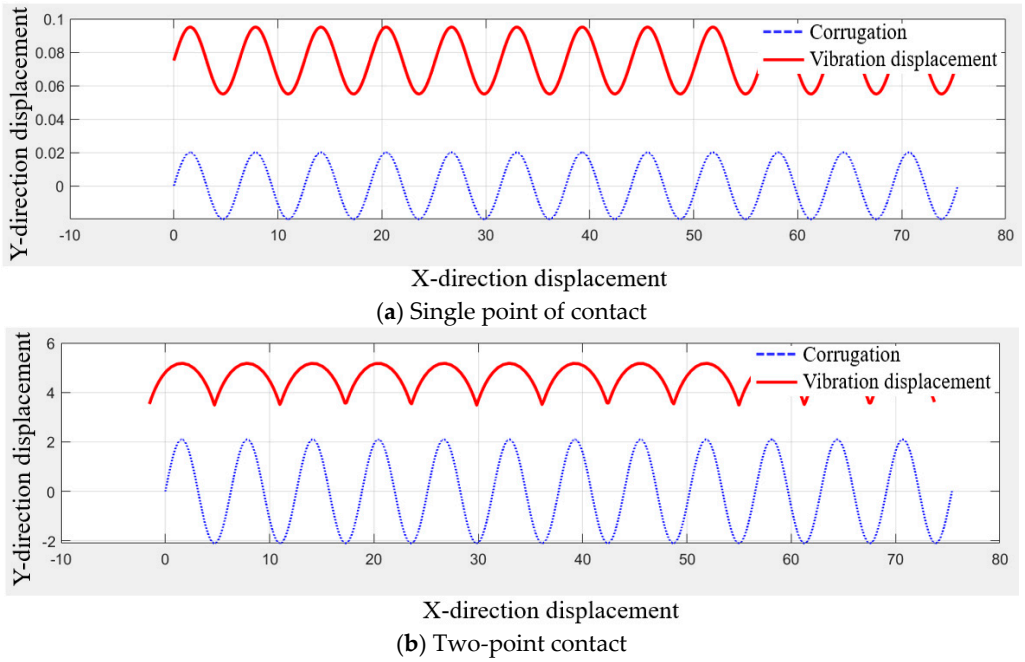
$$y_a = \frac{A^2 {R_{nV}}^4 W^5 \cos(n_V W_t)^2}{\left(A^2 {n_V}^2 W^2 \cos(n_V W_t)^2 + W^2\right)^{\frac{3}{2}}} - A {n_V}^2 W^2 \sin(n_V W_t) - \frac{A^2 {R_{nV}}^4 W^5 \sin(n_V W_t)^2}{\left(A^2 {n_V}^2 W^2 \cos(n_V W_t)^2 + W^2\right)^{\frac{3}{2}}} + \frac{3A^4 {R_{nV}}^6 W^7 \cos(n_V W_t)^2 \sin(n_V W_t)^2}{\left(A^2 {n_V}^2 W^2 \cos(n_V W_t)^2 + W^2\right)^{\frac{5}{2}}} \tag{4}$$

Equation (5) for finding the derivative of vibration acceleration.

$$dy_a = \frac{9A^4 {R_{nV}}^7 W^8 \cos(n_V W_t)^3 \sin(n_V W_t)}{\left(A^2 {n_V}^2 W^2 \cos(n_V W_t)^2 + W^2\right)^{\frac{5}{2}}} - \frac{4A^2 {R_{nV}}^5 W^6 \cos(n_V W_t) \sin(n_V W_t)}{\left(A^2 {n_V}^2 W^2 \cos(n_V W_t)^2 + W^2\right)^{\frac{3}{2}}} + \frac{9A^4 {R_{nV}}^7 W^8 \cos(n_V W_t) \sin(n_V W_t)^3}{\left(A^2 {n_V}^2 W^2 \cos(n_V W_t)^2 + W^2\right)^{\frac{5}{2}}} - A {n_V}^3 W^2 \cos(n_V W_t) + \frac{15A^6 {R_{nV}}^9 W^{10} \cos(n_V W_t)^3 \sin(n_V W_t)^3}{\left(A^2 {n_V}^2 W^2 \cos(n_V W_t)^2 + W^2\right)^{\frac{7}{2}}} \tag{5}$$

In Equation (5), when x is an integer multiple of $\pi/2$, the formula value is 0. That is, the maximum value of vibration acceleration occurs at the integer multiple of $\pi/2$.

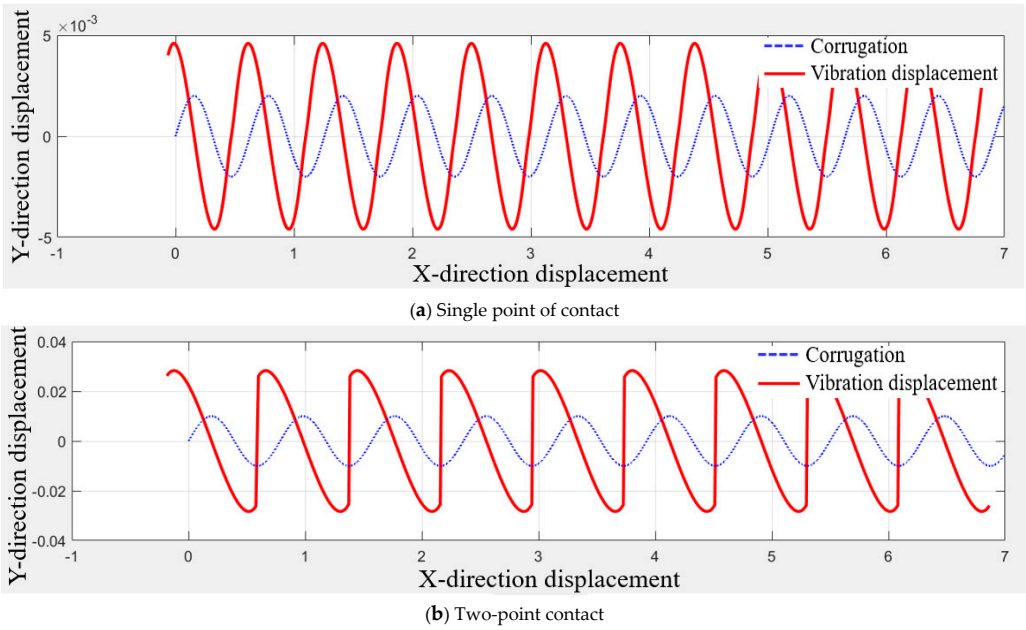
Figure 2 is a schematic diagram of the vibration displacement of single-point and two-point contact. Figure 3 is a schematic diagram of the contact velocity between the ball and the waviness of single-point and two-point contact. Figure 4 is a schematic diagram of the contact acceleration between the ball and the waviness of single-point and two-point contact. Figure 5 is a partially enlarged schematic diagram of the ball and the waviness of single-point and two-point contact.



(**a**) Single point of contact

(**b**) Two-point contact

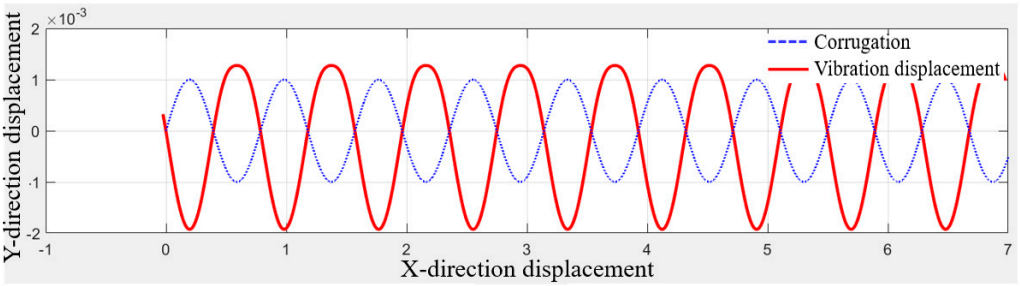
Figure 2. Vibration displacement in the time domain.



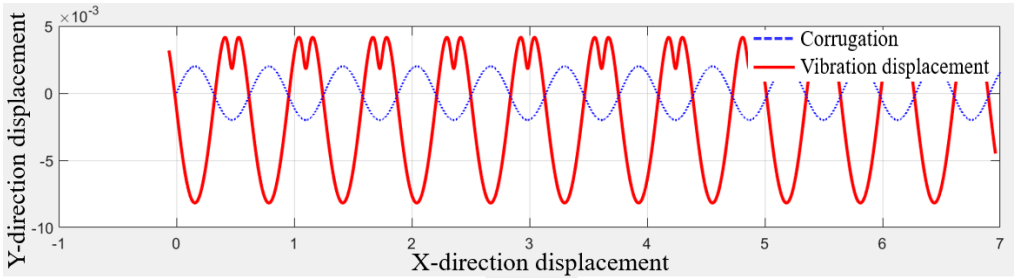
(**a**) Single point of contact

(**b**) Two-point contact

Figure 3. Time-domain of the contact vibration velocity between the ball and the waviness.

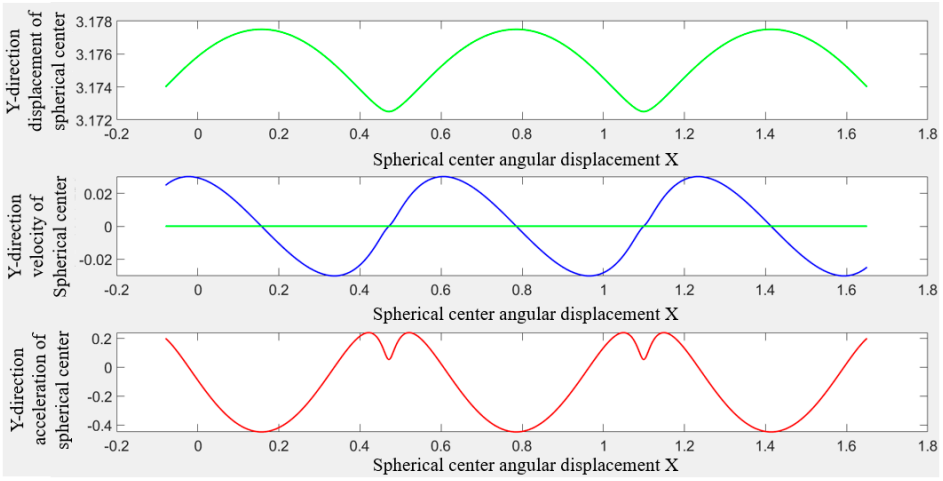


(**a**) Single point of contact

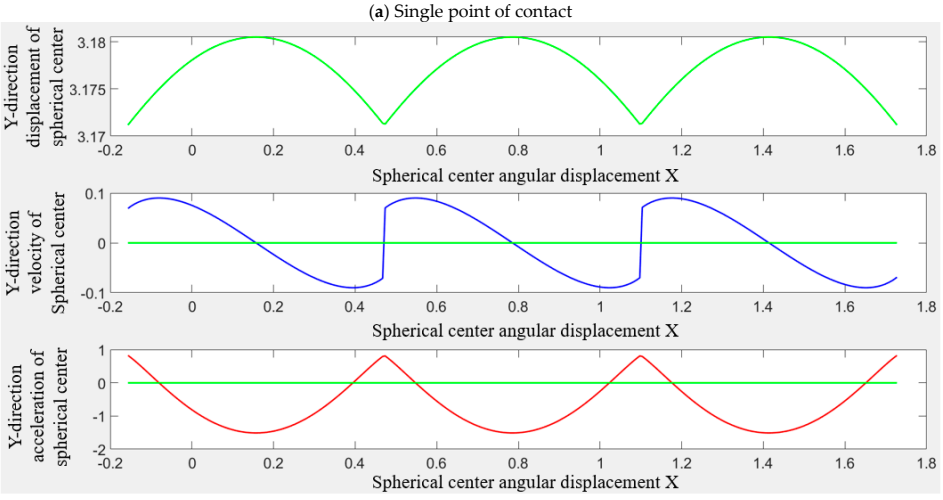


(**b**) Two-point contact

Figure 4. Time-domain of vibration acceleration in contact between a ball and waviness.



(**a**) Single point of contact



(**b**) Two-point contact

Figure 5. Local amplification time domain of vibration parameters in contact between a ball and waviness.

2.3. Excitation Sensitivity Model

Because vibration acceleration can more accurately reflect the influence of surface waviness, this study focused on analyzing the relationship between vibration acceleration and surface waviness and vibration. From the vibration acceleration Equation (4), the waviness amplitude a, the waviness order n_v, and the spherical radius R all have an influence on the vibration acceleration [43–45].

By calculating the partial derivative of vibration acceleration Equation (4) relative to ripple amplitude A, we can obtain the sensitivity of ripple amplitude A to the influence of vibration acceleration (Equation (6)) [46–48].

$$dA = \frac{2AR_{nV}{}^4W^5\cos(n_VW_t)^2}{\left(A^2n_V{}^2W^2\cos(n_VW_t)^2+W^2\right)^{\frac{3}{2}}} - \frac{3A^3R_{nV}{}^6W^7\cos(n_VW_t)^2}{\left(A^2n_V{}^2W^2\cos(n_VW_t)^2+W^2\right)^{\frac{5}{2}}} - n_V{}^2W^2\sin(n_VW_t) - \frac{2AR_{nV}{}^4W^5\sin(n_VW_t)^2}{\left(A^2n_V{}^2W^2\cos(n_VW_t)^2+W^2\right)^{\frac{3}{2}}} + \frac{15A^3R_{nV}{}^6W^7\cos(n_VW_t)^2\sin(n_VW_t)^2}{\left(A^2n_V{}^2W^2\cos(n_VW_t)^2+W^2\right)^{\frac{5}{2}}} - \frac{15A^5R_{nV}{}^8W^9\cos(n_VW_t)^4\sin(n_VW_t)^2}{\left(A^2n_V{}^2W^2\cos(n_VW_t)^2+W^2\right)^{\frac{7}{2}}} \quad (6)$$

In the same way, the partial derivatives n_v, R, and W can also be calculated for the vibrational acceleration to obtain the sensitivity coefficients of the influence of n_v, R, and W on the vibrational acceleration. It is worth noting that the mode approximates a sinusoidal waveform and does not take into account multiple harmonic components, random ripples, load distribution, clearance, lubrication, cage dynamics, and installation errors. Actual bearing surface corrugation usually contains multi-order harmonics, random components, and local inhomogeneity. A single sine wave cannot fully represent the real topography, but it can be used as the smallest explainable unit of corrugation excitation for mechanism analysis and parameter sensitivity research.

2.4. Vibration Test System

According to the industry standard of rolling bearing vibration measurement, during the measurement, the inner ring of the bearing under test rotates with the main shaft, while the outer ring remains macroscopically stationary. Under the condition of applying a certain external load, the radial vibration value of the outer ring of the bearing was picked up by a speed or acceleration sensor. The vibration sensor was fixed on the measuring rod through bolt connection, one end of the measuring rod was connected with the spring, and the other end was in contact with the outer ring of the bearing being measured. During measurement, the vibration of the outer ring excited the measuring rod, thus forming a mass-spring-contact pair system with sensors [49–53]. Figure 6 is a schematic diagram of the principle of bearing contact vibration detection.

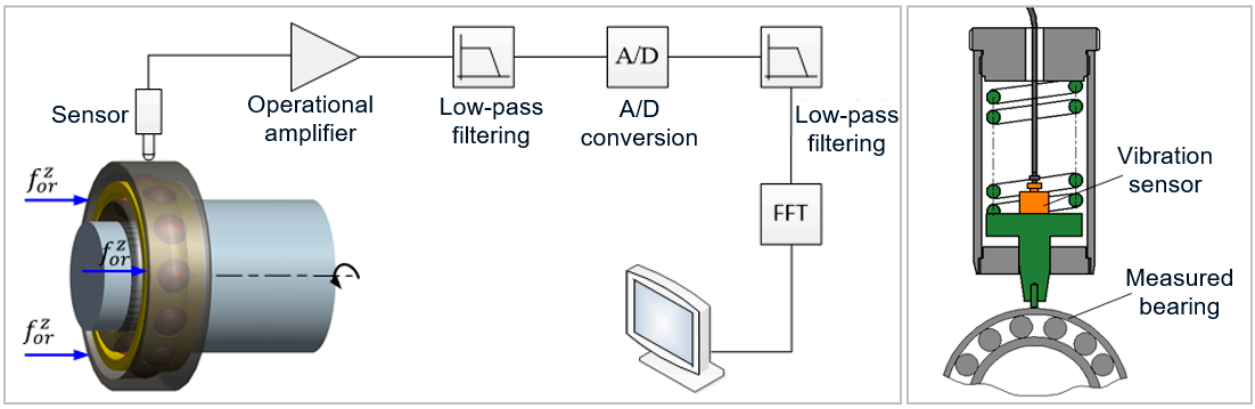


Figure 6. Bearing contact vibration detection principle.

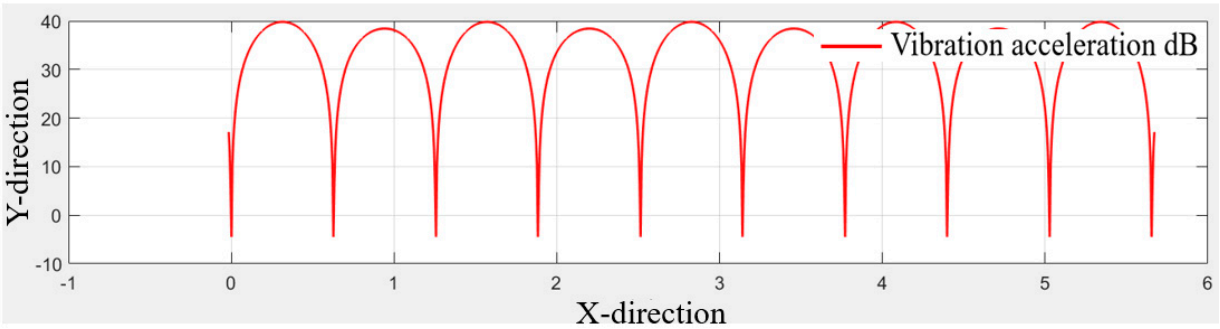
Before measurement, the bearing to be tested was cleaned and air dried, and lubricating oil applied. It was then mounted on the spindle of the drive device and an axial load was applied. The position of the sensor rod was adjusted so that it was in contact with the outer ring of the bearing. The contact point was located halfway across the width of the outer ring cylindrical surface. During the measurement, the spindle speed was 1800 r/min and the axial load was 200 N. The data was saved after the vibration signal stabilized.

Under high-speed conditions, the influence of vibration acceleration on bearing performance was more significant and intuitive. Therefore, vibration acceleration was generally used to measure the vibration performance of high-speed angular contact ball bearings. Its calculation formula was Equation (7).

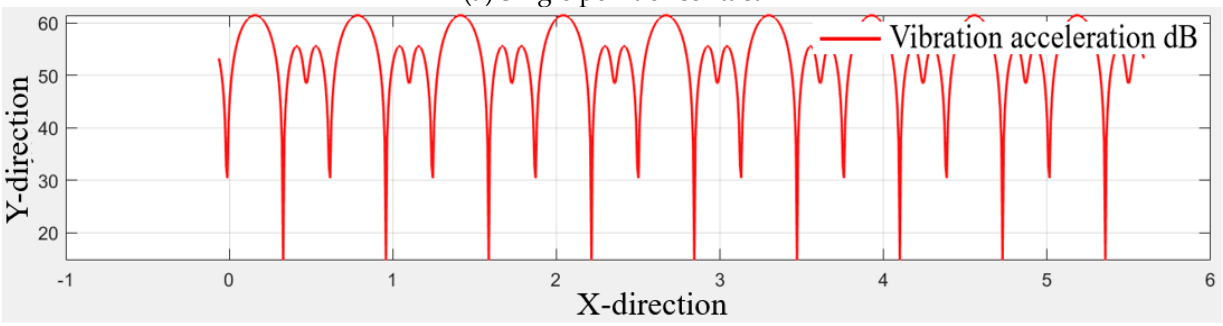
$$y_a = 20\lg\frac{y_{rms}}{g} \tag{7}$$

where y_{rms} is the root mean square of the vibrational acceleration within a certain frequency range, where the frequency range was usually 50~10,000 Hz; g is the gravitational acceleration, whose value is 9.81×10^{-3} m/s^2. The value of y_a is the comprehensive vibration level of the bearing under test.

The bearing vibration acceleration was calculated according to Equation (4), and the bearing vibration results measured by the vibration acceleration tester can be predicted by incorporating it into Equation (7). Figure 7 is a schematic diagram of the vibration acceleration test prediction for single-point and two-point contact.



(**a**) Single point of contact



(**b**) Two-point contact

Figure 7. Schematic diagram of vibration acceleration test prediction.

3. Analysis of Influencing Factors

Based on the basic parameters of angular contact ball bearing 7008/P4, the effects of the contact between the bearing ball and the raceway waviness, the waviness amplitude A and order n_v, the rotational speed v and the ball diameter D_w on the vibration of rolling bearings were studied. The basic parameters of the bearing 7008/P4 were shown in Table 1.

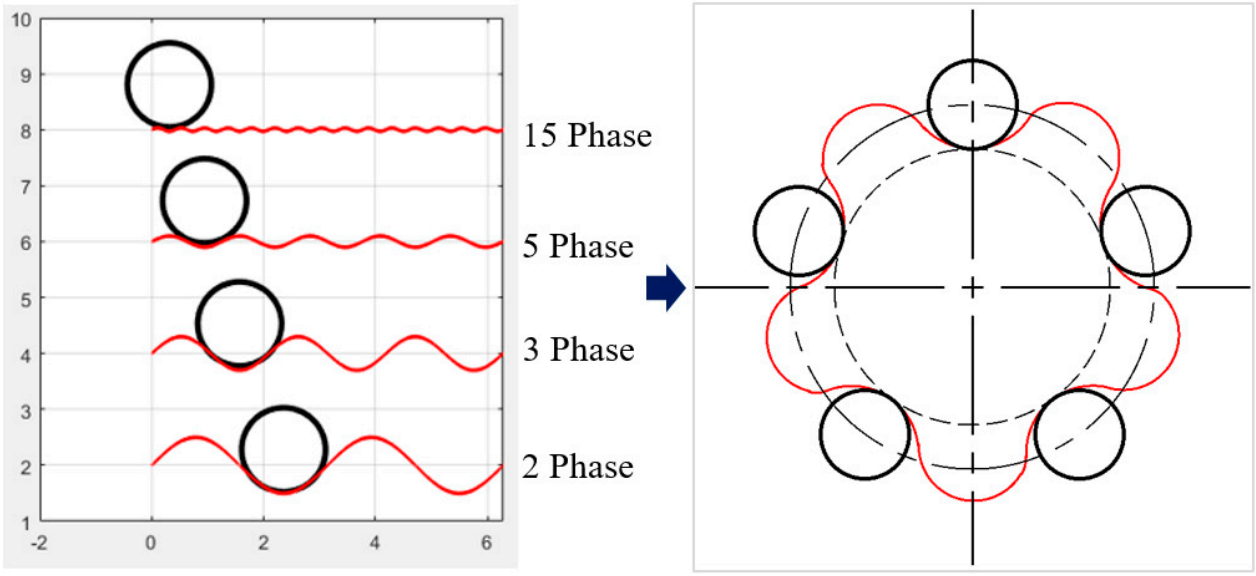
Table 1. Basic parameters of bearing 7008/P4.

Parameter	Value	Unit
Outer ring diameter D	68	mm
Inner ring diameter d	40	mm
Width T	15	mm
Outer ring channel diameter D_e	61.964	mm
Inner ring channel diameter d_i	47.616	mm
Ball diameter D_w	6.35	mm
Number of balls Z	8	
Contact angle a	15	°
Vibration measurement rotation speed n_i	1800	R/min

From Equations (1) to (7), given a constant sphere diameter, the order and amplitude of the surface waviness match when a single point comes into contact with the critical value. Table 2 shows the matching of several important orders and amplitudes of the surface waviness when a critical single point makes contact. Figure 8 is a schematic diagram.

Table 2. Matching of importance order and amplitude.

Order n_v	2	3	5	15
Amplitude A (μm)	78.740	34.996	12.598	1.40



(**a**) Matching different orders and amplitudes (**b**) Matching typical 5th orders and amplitudes

Figure 8. Matching ripple order and amplitude.

3.1. Impact of Amplitude

3.1.1. Influence of Amplitude on Vibration

The bearing ball diameter $D_w = 6.35$ mm and the waviness order $n_v = 10$. As can be seen from Equation (6), when the waviness amplitude $A = 0.0032$, the ball and the waviness are in exact single-point contact. Therefore, values were taken on both sides of the waviness amplitude $A = 0.0032$ to observe the influence of the waviness on bearing vibration. The influence of the waviness amplitude on bearing vibration is shown in Table 3.

Table 3. Influence of waviness amplitude on bearing vibration.

No.	Amplitude A (mm)	Maximum Vibration Acceleration (dB)	Remark
1	0.001	53.56	Single point of contact
2	0.0015	58.06	Single point of contact
3	0.002	61.44	Single point of contact
4	0.0025	64.18	Single point of contact
5	0.003	66.5	Single point of contact
6	0.0032	67.34	Contact critical
7	0.0035	68.52	Two-point contact
8	0.004	70.31	Two-point contact
9	0.0045	71.92	Two-point contact
10	0.005	73.38	Two-point contact
11	0.0055	74.72	Two-point contact
12	0.006	75.97	Two-point contact

Figure 9 is a schematic diagram of vibration acceleration corresponding to the case where the amplitude A is a minimum value of 0.001 mm, an intermediate value of 0.003, and a maximum value of 0.006, respectively.

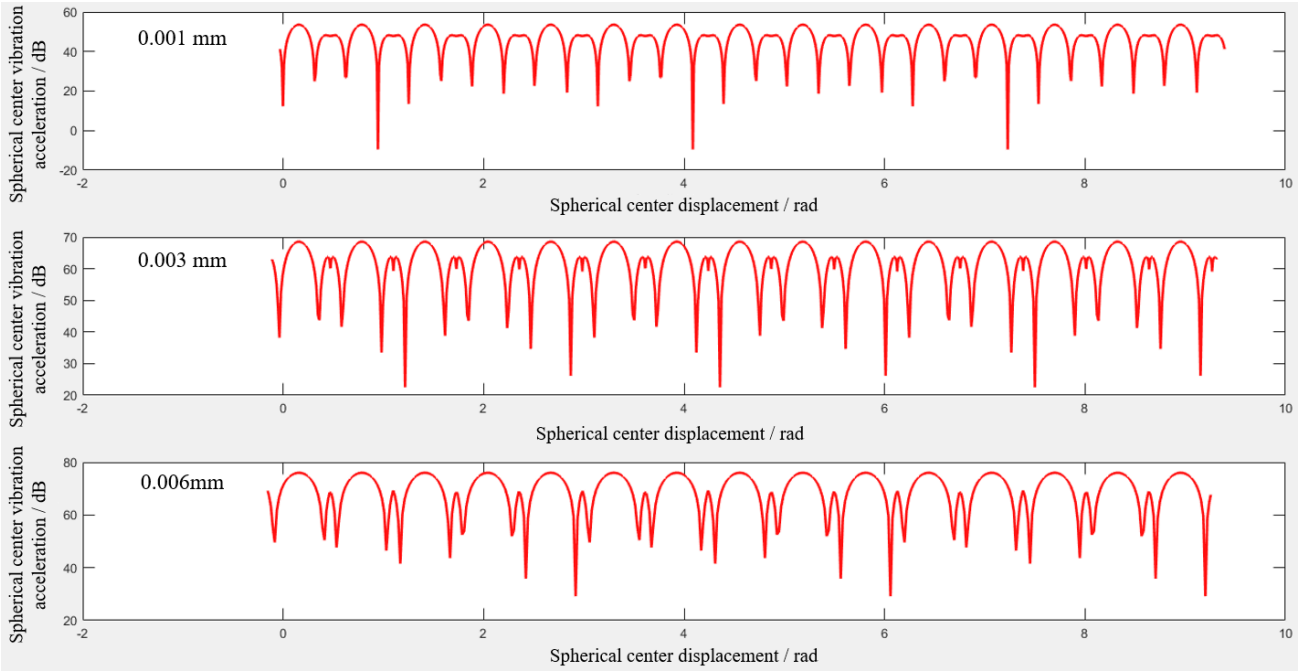


Figure 9. The influence of ripple amplitude on vibration.

To visually display the impact of different amplitudes on bearing vibration acceleration, a trend curve of vibration acceleration as a function of amplitude A is plotted as shown in Figure 10.

For Table 3 and Figure 10, as the amplitude of the ripple increases, the bearing vibration intensifies, and the degree of intensification gradually becomes more moderate. This indicates that as the amplitude increases, its influence on the vibration gradually increases, but the degree of influence weakens. There is no change in vibration acceleration at or near the critical point of single-point contact and two-point contact, indicating that single-point contact and two-point contact have no influence on the maximum vibration acceleration.

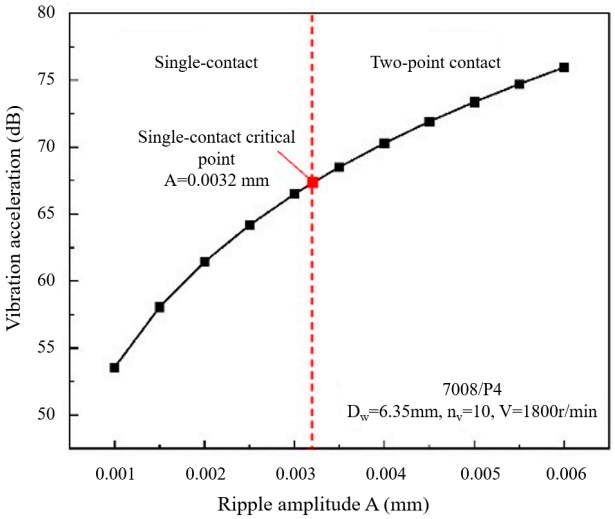


Figure 10. Influence of ripple amplitude on vibration.

3.1.2. Influence of Amplitude on the Sensitivity of Each Factor

Assuming that the bearing ball diameter $D_w = 6.35$ mm, the waviness order $n_v = 5$, and the rotation speed $v = 1800$ r/min remain unchanged, according to Equations (1)–(7), the sensitivity of each factor to bearing vibration at different waviness amplitudes can be obtained under the condition of maximum vibration acceleration. A bar comparison chart and trend curve of the sensitivity of each factor changing with the amplitude A are drawn as shown in Figure 11.

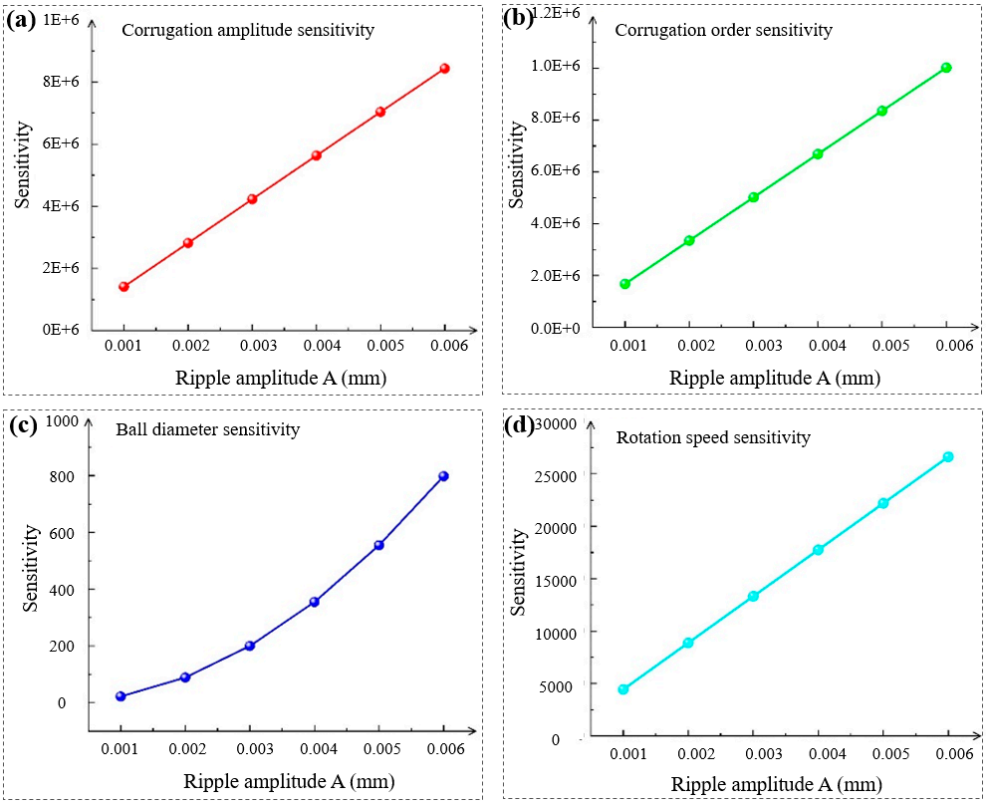


Figure 11. The influence trend of amplitude on the sensitivity of various factors. (**a**) Corrugation amplitude sensitivity; (**b**) Corrugation order sensitivity; (**c**) Ball diameter sensitivity; (**d**) Rotation speed sensitivity.

For Figure 11, as the waviness amplitude increases, the sensitivity of the bearing's waviness amplitude A, waviness order n_v, bearing ball diameter Dw, and bearing speed v to vibration all increase. However, the sensitivity of the bearing's waviness amplitude A, waviness order n_v, and bearing speed v to vibration remains unchanged, while the sensitivity of the bearing's ball diameter D_w increases with the increase in amplitude.

To more intuitively compare the sensitivity of each parameter to vibration as it changes with amplitude, the average of the sensitivities of each parameter is calculated, and the sensitivity of the sphere diameter is used as a reference. The sensitivity of each parameter is divided by the sensitivity of the sphere diameter to obtain a dimensionless value for the sensitivity comparison, as shown in Table 4.

Table 4. Comparison of mean sensitivity values of each factor with amplitude change.

Sensitivity	The Sensitivity Corresponding to Each Parameter Changes with Amplitude			
	Amplitude *A*	**Order n_v**	**Ball Diameter *R***	**Angular Velocity *w***
Mean value	492,765.3	585,164	336.5	15,533.2
Dimensionless value	1464	1738	1	46

For Table 4, as the waviness amplitude increases, the influence of bearing waviness amplitude A, waviness order n_v, bearing ball diameter D_w, and bearing speed v on vibration varies greatly. The influence of ball diameter was the smallest, and the influence of waviness order was the greatest. The average sensitivity was 1738 times that of ball diameter; the influence of waviness amplitude was also greater, 1464 times that of ball diameter; and the influence of bearing speed was smaller, 46 times that of ball diameter.

3.2. Influence of Order

3.2.1. Effect of Order on Vibration

Bearing ball diameter $D_w = 6.35$ mm, waviness amplitude $A = 0.0032$, $v = 1800$ r/min. For Equation (6), when the waviness order $n_v = 10$, the sphere and the waviness were in exact single-point contact. Therefore, values were taken on both sides of the waviness order $n_v = 10$, and the influence of the waviness order n_v on bearing vibration was observed. The trend curve of vibration acceleration changing with the order n_v was plotted as shown in Figure 12.

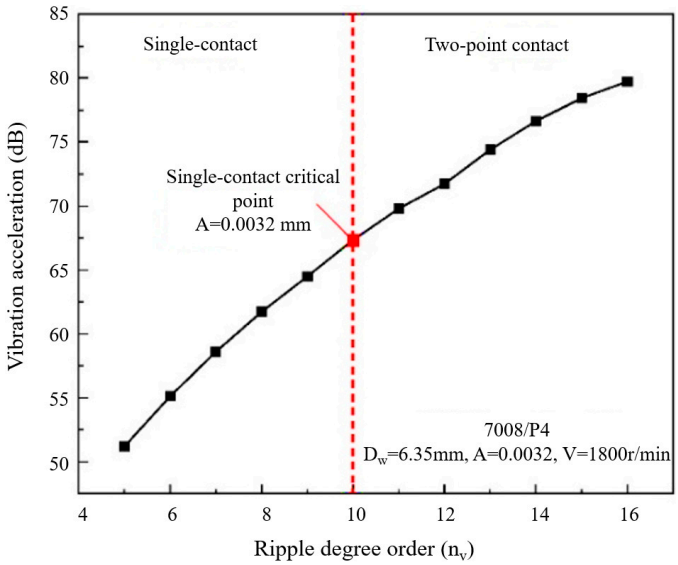


Figure 12. Influence of waviness order on vibration.

For Figure 12, as the waviness order increases, the bearing vibration intensifies, but the degree of intensification remains basically unchanged, indicating that the degree of its influence on vibration remains unchanged as the order increases. There was no change in vibration acceleration at or near the critical point of single-point contact and two-point contact, indicating that single-point contact and two-point contact have no influence on the maximum vibration acceleration.

3.2.2. Influence of Order on the Sensitivity of Each Factor

Bearing ball diameter $Dw = 6.35$ mm, waviness amplitude $A = 0.0032$ mm, $v = 1800$ r/min. According to Equations (1)–(7), the sensitivity of each factor to bearing vibration when taking different waviness orders can be obtained under the condition of maximum vibration acceleration. The calculation results are shown in Table 5.

Table 5. Sensitivity of each factor at different ripple amplitudes.

No.	Order n_v	Amplitude A Sensitivity	Order n_v Sensitivity	Ball Diameter R Sensitivity	Angular Velocity w Sensitivity
1	5	450,892	535,211	227	14,205
2	6	934,654	770,538	471	24,543
3	7	1,730,870	1,048,562	873	38,969
4	8	2,951,428	1,369,256	1489	58,163
5	9	4,725,151	1,732,592	2384	82,805
6	10	7,197,676	2,138,543	3633	113,575
7	11	10,531,327	2,587,083	5316	151,152
8	12	14,904,960	3,078,183	7527	196,216
9	13	20,513,799	3,611,817	10,364	249,445
10	14	27,569,260	4,187,959	13,935	311,517
11	15	36,298,755	4,806,581	18,355	383,111
12	16	46,945,481	5,467,658	23,750	464,906

For Table 5, as the waviness order increases, the sensitivity of the bearing's waviness amplitude A, waviness order n_v, bearing ball diameter D_w, and bearing speed v to vibration all increase, and the sensitivity becomes greater as the order increases.

To more intuitively compare the sensitivity of each parameter to vibration as a function of order, the average sensitivity of each parameter is calculated, and the sensitivity of the sphere diameter is used as a reference. The sensitivity of each parameter is divided by the sensitivity of the sphere diameter to obtain a dimensionless value for the sensitivity comparison, as shown in Table 6.

Table 6. Comparison of average sensitivity values of each factor with order change.

Sensitivity	Sensitivity Corresponding to Each Parameter Varies with Order			
	Amplitude A	Order n_v	Ball Diameter R	Angular Velocity w
Mean value	14,562,854.42	2,611,165.25	7360.33	174,050.58
Dimensionless value	1978	354	1	23

For Table 6, as the waviness order increases, the influence of bearing waviness amplitude a, waviness order n_v, bearing ball diameter D_w, and bearing speed v on vibration varies greatly. The influence of ball diameter was the smallest, while the influence of waviness amplitude was the largest, which was 1978 times that of ball diameter. Other influences were smaller. The average sensitivity of waviness order was 354 times that of ball diameter, and the bearing speed was 23 times that of ball diameter.

3.3. Influence of Ball Diameter

3.3.1. Influence of Ball Diameter on Vibration

The waviness n amplitude $A = 0.0032$, the waviness order $n_v = 10$, and the rotation speed $v = 1800$ r/min. For Equation (6), when the bearing ball diameter $D_w = 6.35$ mm, the ball and the waviness were in exact single-point contact. Therefore, values were taken on both sides of the ball diameter $D_w = 6.35$ mm to see the influence of waviness on bearing vibration. The calculation results are shown in Table 7.

Table 7. Influence of ripple amplitude on bearing vibration.

No.	Ball Diameter D_w (mm)	Maximum Vibration Acceleration dB	Remark
1	2	63.68	Single point of contact
2	3	64.67	Single point of contact
3	4	65.55	Single point of contact
4	5	66.36	Single point of contact
5	6	67.10	Single point of contact
6	6.35	67.34	Contact critical
7	7	67.78	Two-point contact
8	8	68.41	Two-point contact
9	9	69.00	Two-point contact
10	10	69.55	Two-point contact
11	11	70.06	Two-point contact
12	12	70.55	Two-point contact

To visually display the impact of different ball diameters on bearing vibration acceleration, a trend curve of vibration acceleration versus ball diameter D_w was plotted as shown in Figure 13.

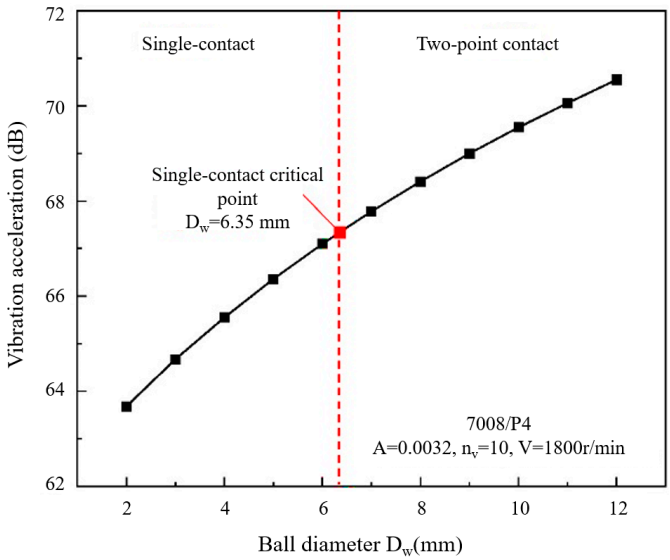


Figure 13. Effect of bearing ball diameter on vibration.

For Table 7 and Figure 13, bearing vibration intensifies as the ball diameter of the bearing increases, but the degree of intensification remains basically unchanged, indicating that the degree of influence on vibration remains unchanged as the ball diameter increases. There was no change in vibration acceleration at or near the critical point of single-point contact and two-point contact, indicating that single-point contact and two-point contact have no influence on the maximum vibration acceleration.

3.3.2. Influence of Ball Diameter on Sensitivity of Various Factors

The waviness amplitude $A = 0.0032$ mm, the waviness order $n = 10$, and the rotation speed $v = 1800$ r/min. According to Equations (1)–(7), the sensitivity of each factor to bearing vibration under the condition of maximum vibration acceleration can be obtained by taking different ball diameters (set as a series of positive integers for ease of study). The calculation results are shown in Table 8.

Table 8. Sensitivity of various factors at different sphere radii.

No.	Ball Diameter R (mm)	Amplitude A Sensitivity	Order n_v Sensitivity	Ball Diameter R Sensitivity	Angular Velocity w Sensitivity
1	3	6,800,953	2,138,797	3632	113,582
2	4	9,067,938	2,137,345	3632	113,543
3	5	11,334,923	2,135,893	3632	113,505
4	6	13,601,907	2,134,441	3632	113,466
5	7	15,868,892	2,132,989	3632	113,428
6	8	18,135,877	2,131,537	3632	113,389
7	9	20,402,861	2,130,085	3632	113,350
8	10	22,669,846	2,128,633	3632	113,312

For Table 8, as the ball diameter increases, the sensitivity of the bearing waviness amplitude A to vibration increases, the sensitivity of waviness order n_v and the bearing speed v to vibration both decrease, and the sensitivity of the bearing ball diameter D_w to vibration remains unchanged.

To more intuitively compare the sensitivity of each parameter to vibration as it changes with amplitude, the average of the sensitivities of each parameter was calculated, and the sensitivity of the sphere diameter was used as a reference. The sensitivity of each parameter was divided by the sensitivity of the sphere diameter to obtain a dimensionless value for the sensitivity comparison, as shown in Table 9.

Table 9. Comparison of average sensitivity values of various factors with changes in sphere diameter.

Sensitivity	The Sensitivity Corresponding to Each Parameter Varies with Order			
	Amplitude A	Order n_v	Ball Diameter R	Angular Velocity w
Mean value	14,735,400	2,133,715	3632	113,446.875
Dimensionless value	4057	587	1	31

For Table 9, as the waviness order increases, the sensitivity of bearing waviness amplitude a, waviness order n_v, bearing ball diameter D_w, and bearing speed v to vibration varies greatly. The influence of ball diameter was the smallest, while the influence of waviness amplitude was the largest, which was 4057 times that of ball diameter. Other influences were smaller. The average sensitivity of the waviness order was 587 times that of ball diameter, and the bearing speed was 31 times that of ball diameter.

3.4. Influence of Rotational Speed

3.4.1. Influence of Rotational Speed on Vibration

The bearing ball diameter $D_w = 6.35$ mm, the waviness order $n = 10$, and the waviness amplitude $A = 0.0032$. For Equation (6), when the rotation speed $v = 1800$ r/min, the ball and the waviness were in exact single-point contact. Therefore, values were taken on both sides of the rotational speed $v = 1800$ r/min to see the influence of surface waviness on bearing vibration, and the trend curve of vibration acceleration changing with bearing rotational speed v is plotted as shown in Figure 14.

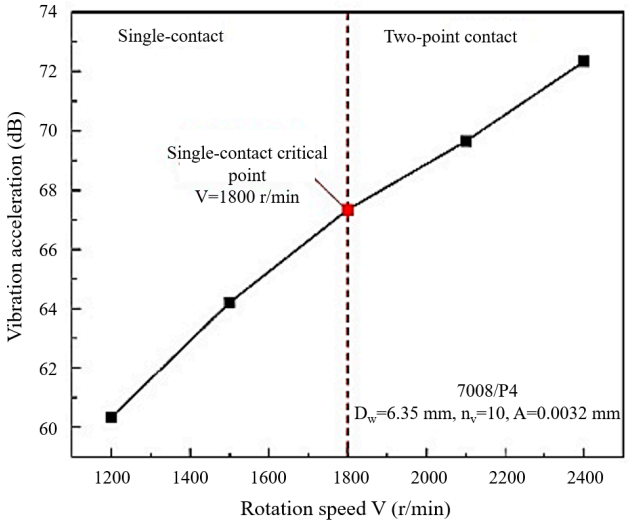


Figure 14. Effect of bearing speed on vibration.

For Figure 14, the bearing vibration intensifies as the rotation speed increases, but the degree of intensification remains basically unchanged, indicating that the degree of its influence on vibration remains unchanged as the rotation speed increases. There is no change in vibration acceleration at or near the critical point of single-point contact and two-point contact, indicating that single-point contact and two-point contact have no influence on the maximum vibration acceleration.

3.4.2. Influence of Rotational Speed on Sensitivity of Various Factors

The bearing ball diameter D_w = 6.35 mm, the waviness amplitude A = 0.0032 mm, and the waviness order n_v = 10. According to Equations (1)–(7), the sensitivity of each factor to bearing vibration at different rotational speeds can be obtained under the condition of maximum vibration acceleration. The calculation results are shown in Table 10.

Table 10. Sensitivity of each factor at different rotational speeds.

No.	Rotation Speed n (rpm)	Amplitude A Sensitivity	Order n_v Sensitivity	Ball Diameter R Sensitivity	Angular Velocity w Sensitivity
1	1200	3,198,967	632,959	1614	50,450
2	1500	4,998,386	1,237,049	2522	78,854
3	1800	7,197,676	2,138,543	3632	113,575
4	2100	9,796,837	3,396,974	4944	154,612
5	2400	12,795,868	5,071,872	6458	201,966

For Table 10, as the waviness order increases, the sensitivity of the bearing's waviness amplitude A, waviness order n_v, bearing ball diameter D_w, and bearing speed v to vibration all increases, and the sensitivity becomes greater as the order increases.

To more intuitively compare the sensitivity of each parameter to vibration as it changes with amplitude, the average of the sensitivities of each parameter is calculated, and the sensitivity of the sphere diameter is used as a reference. The sensitivity of each parameter is divided by the sensitivity of the sphere diameter to obtain a dimensionless value for the sensitivity comparison, as shown in Table 11.

For Table 11, as the waviness order increases, the sensitivity of bearing waviness amplitude a, waviness order n_v, bearing ball diameter D_w, and bearing speed v to vibration varies greatly. The influence of ball diameter was the smallest, while the influence of waviness amplitude was the largest, which was 1981 times that of ball diameter. Other

influences were smaller. The average sensitivity of waviness order was 650 times that of ball diameter, and the bearing speed was 31 times that of ball diameter.

Table 11. Comparison of average sensitivity values of various factors as a function of rotational speed.

Sensitivity	The Sensitivity Corresponding to Each Parameter Varies with Order			
	Amplitude A	Order n_v	Ball Diameter R	Angular Velocity w
Mean value	7,597,546.8	2,495,479.4	3834	119,891.4
Dimensionless value	1981	650	1	31

4. Vibration Prediction and Model Verification

Taking 7008C/P4 as an object, five inner rings of this model of bearing were selected for coarse grinding, fine grinding, and ultra-fine grinding, respectively. In addition, five inner rings after ultra-fine grinding were selected for force-rheological polishing. During the experiment, many scholars also studied various sensors [54–56], thereby analyzing the surface roughness after final polishing. The principle of force-rheological polishing and the comparison of the surface quality of the front and rear bearings are shown in Figure 15.

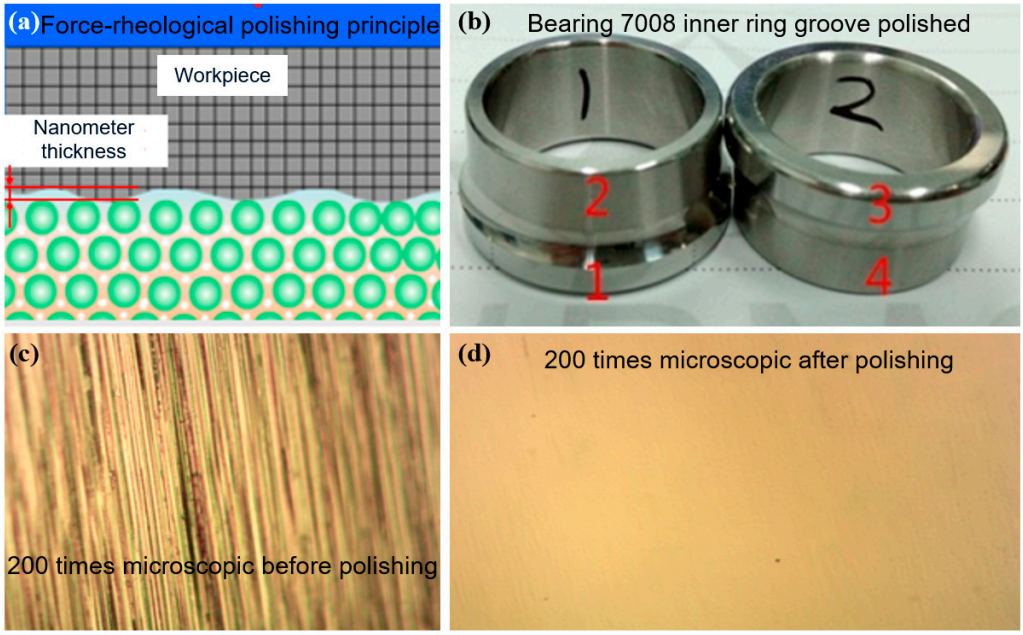


Figure 15. Principle of force-rheological polishing and surface quality of front and rear bearings. (**a**) Force-rheological polishing principle; (**b**) Bearing 7008 inner ring groove polished; (**c**) 200 times microscopic before polishing; (**d**) 200 times microscopic after polishing.

For the outer ring, finished outer rings with basically consistent waviness accuracy after ultra-precision were selected. High-precision steel balls (G5) were selected for the rolling elements, and four sets of five sets of bearings each were assembled for a total of 20 sets of bearings. Because the accuracy of bearing balls is high and the accuracy of the outer ring of the bearing is basically consistent, the influence of the surface quality of the outer ring and the steel ball on bearing vibration was negligible. Meanwhile, in order to reduce the workload, this paper only takes the 15th order of surface waviness and its amplitude as an example for illustration. The detection records of the ripple amplitudes for each group are shown in Table 12, where Av is the measured average. Figure 16a,b show the measurement of the bearing inner ring and waviness amplitude in different processes. Figure 16c is bearing vibration acceleration tester. Figure 16(c-1),(c-2),(c-3),(c-4) are time domain signals for different processes.

Table 12. Bearing waviness amplitude test record.

Process	A15 Test Record (μm)					A_v (μm)
	1	2	3	4	5	
Coarse grinding	0.261	0.312	0.246	0.281	0.321	0.284
Fine grinding	0.156	0.183	0.149	0.211	0.168	0.173
Ultra-precision grinding	0.065	0.062	0.056	0.049	0.055	0.057
Polishing	0.008	0.011	0.016	0.009	0.012	0.011

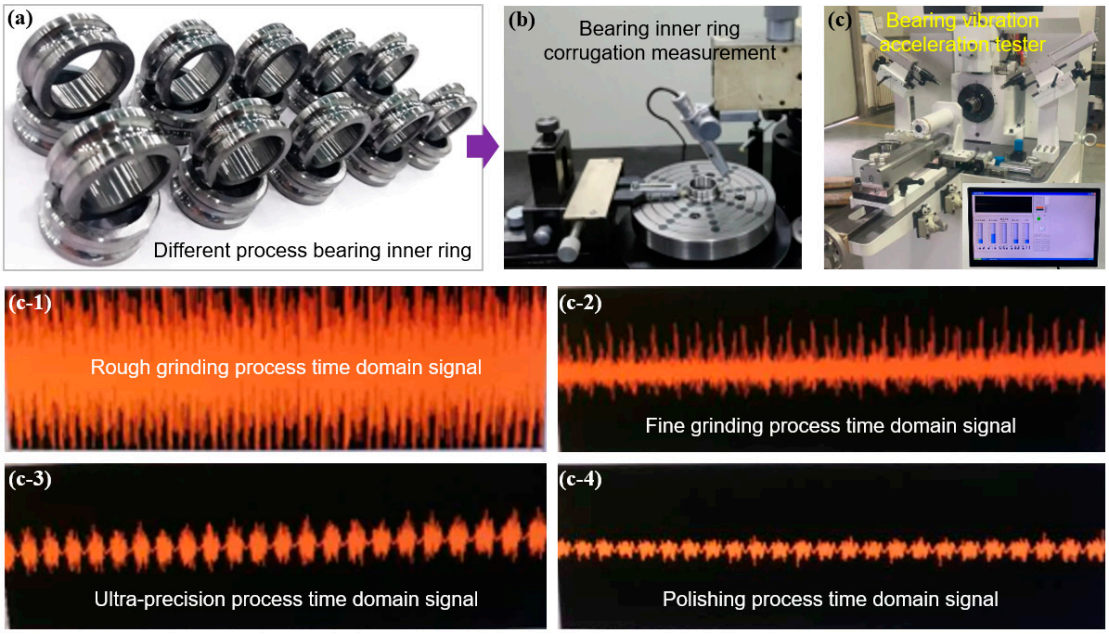


Figure 16. Comprehensive data measurement results under different processes.

Assuming the rotation speed v = 1800 rpm, the vibration acceleration corresponding to the waviness amplitude value detected in each process was calculated using a model, as shown in Table 13, where G_v is the average value of the vibration acceleration calculation.

Table 13. Vibration acceleration values of bearing 7008.

Process	A15 Test Record (dB)					G_v (dB)
	G1	G2	G3	G4	G5	
Coarse grinding	53.046	54.859	52.453	53.792	55.152	53.860
Fine grinding	48.009	49.545	47.571	50.934	48.719	48.956
Ultra-precision grinding	39.881	39.453	38.533	37.331	38.371	38.714
Polishing	21.339	24.124	27.409	22.369	24.886	24.025

The bearings after four processes were tested using a precision bearing vibration accelerometer. The rotation speed v of the detector S0910C(ZYS, CHINA, group standards) was 1800 rpm. The test results are shown in Table 14, where Gv0 is the average value of the vibration acceleration detection.

As shown in Tables 13 and 14, as the machining precision increases and the surface quality of the bearing ring improves; the bearing vibration value also decreases significantly, and the deviation range of the vibration acceleration time domain signal also becomes significantly narrower and more uniform, as shown in Figure 16(c-1),(c-2),(c-3),(c-4). Table 15 shows the comparison and relative error between the calculated average of the model and the actual measured average.

Table 14. Bearing 7008 vibration acceleration values.

Process	A15 Test Record (dB)					G_{v0} (dB)
	G1	G2	G3	G4	G5	
Coarse grinding	54.8	56.6	54.2	55.1	58.9	55.9
Fine grinding	47.8	48.9	48.2	49.6	48.5	48.6
Ultra-precision grinding	36.4	37.2	38.5	36.8	37.4	37.3
Polishing	23.2	24.5	28.4	23.6	25.5	25.0

Table 15. Model calculation results and actual mean error.

Process	Gv (dB)	Gv0 (dB)	Error (100%)
Coarse grinding	53.860	55.9	4
Fine grinding	48.955	48.6	1
Ultra-precision grinding	38.713	37.3	4
Polishing	24.025	25.1	4

For Table 15, the waviness amplitudes detected in each process and the corresponding vibration model's calculated vibration values are basically consistent with the trend of changes in the actual detected vibration values. According to [1 − (max predicted value/max actual value)] × 100% = max mean error. The maximum average phase difference error does not exceed 5%, and the vibration analysis model calculation results are correct and highly accurate.

5. Conclusions

This study conducts in-depth research on the relationship between surface waviness and bearing vibration of angular contact ball bearings, obtains the influence law of waviness on bearing vibration, and proposes a precision angular contact ball bearing vibration prediction method and optimization control strategy based on the order and amplitude of waviness. The main research conclusions are as follows:

(1) Based on the relationship between the sinusoidal wave model of corrugation and the motion trajectory of the spherical center, this paper establishes a waviness excitation model and analyzes the excitation mechanism. During measurement, the inner ring of the bearing under test rotates with the main shaft, while the outer ring remains macroscopically stationary. Under the condition of applying a certain external load, the vibration value of the outer ring of the bearing along the radial direction is picked up by a velocity or acceleration sensor. Meanwhile, a bearing vibration acceleration analysis model based on waviness degree and a quantitative calculation method for the influence of the order and amplitude of waviness degree on vibration are given.

(2) Based on the basic parameters of angular contact ball bearing 7008/P4, this paper presents a bearing vibration prediction method and optimization control model based on waviness amplitude and order, and studies the influence of waviness-induced contact excitation between balls and raceway, waviness amplitude A and order n_v, rotational speed v and ball diameter D_w on rolling bearing vibration. The results show that the amplitude of waviness has the greatest influence on vibration, followed by the order of waviness, and the influence is more significant with the increase of rotational speed.

(3) Taking the angular contact ball bearing 7008/P4 as an example, the experiment verified the different waviness states of the four processes of coarse grinding, fine grinding, ultra-precision grinding and polishing. The error between the model calculation results and the actual test results is no more than 5%, which has good accuracy and practicality.

Author Contributions: B.S. and D.W.: Writing—original draft. N.J., Y.G. and Y.S.: Writing—review & editing, Formal analysis. L.H.: Methodology, Conceptualization. All authors have read and agreed to the published version of the manuscript.

Funding: This research was funded by the National Natural Science Foundation of China (52505496), (52675601); Open Project of Anhui Province Key Laboratory of Critical Friction Pair for Advanced Equipment (LCFP-2512); Postdoctoral Fellowship Program of China Postdoctoral Science Foundation (GZC20250909) and National Key R&D Program of Manufacturing Basic Technology and Key Components (2023YFB2406400).

Data Availability Statement: No new data were created or analyzed in this study. Data sharing is not applicable to this article.

Conflicts of Interest: Author Lai Hu was employed by the company Hefei Bolin Advanced Materials Co., Ltd.; authors Dongfeng Wang and Ning Jin were employed by the company Luoyang Bearing Science and Technology Co., Ltd.; and author Yanjun Guo was employed by the company China Academy of Machinery Science and Technology Group Co., Ltd. The remaining authors declare that this research was conducted in the absence of any commercial or financial relationships that could be construed as a potential conflict of interest.

References

1. Hu, L.; Wang, D.; Heow Pueh, L.; Wang, Z. Fatigue Failure of High Precision Spindle Bearing under Extreme Service Conditions. *Eng. Fail. Anal.* **2024**, *25*, 158. [CrossRef]
2. Yu, G.; Liu, J.; Hu, L.; Jiang, A.; Wang, L. Motion system modeling and acceleration analysis of five-axis hybrid machine tool. *Adv. Eng. Inform.* **2026**, *71*, 104368. [CrossRef]
3. Chen, G.; Yuan, L.; Chen, H.; Dou, C.; Ma, G.; Li, S. Machine tool spindle temperature field parametric modeling and thermal error compensation. *Lubricants* **2025**, *13*, 548. [CrossRef]
4. Liu, J.; Li, H.; Song, C.; Wang, Q.; Ma, W.; Zhang, J. Balancing surface finish and ablation depth in direct laser turning of RB-SiC based on combined IPSO-SVR models with MOAHA-TOPSIS method. *Opt. Laser Technol.* **2026**, *194*, 114440. [CrossRef]
5. Huang, S.; Liu, Z.; Li, Y.; Liu, C. Granular boundary layer induces drilling nonlinearity. *Powder Technol.* **2026**, *474*, 122306. [CrossRef]
6. Hu, L.; Ye, J.; Cui, B.; Wang, Z.; Wang, Y. Prediction and evaluation of the influence of static-dynamic aging wear of grease on life of high performance bearings (HPBs). *Eng. Fail. Anal.* **2025**, *179*, 109829. [CrossRef]
7. Ren, H.; Miao, Z.; Feng, X.; Labidi, A.; Zhao, Y.; Wang, C. Modulating the built-in electric field of S-scheme heterojunction via oxygen vacancies for boosting photocatalytic ciprofloxacin degradation. *Chin. Chem. Lett.* **2026**, *37*, 112557. [CrossRef]
8. Hu, L.; Li, B.; Pueh, L.H.; Wang, Z.; Wang, Y. Effect of single/multi-particle grinding parameters on surface properties of bearing steel GCr15. *Eng. Sci. Technol. An. Int. J.* **2024**, *58*, 101851. [CrossRef]
9. Chen, L.; Wang, Y.; Li, Y.; Zhang, Z.; Xue, Z.; Ban, X.; Hu, C.; Li, H.; Tian, J.; Mu, W.; et al. Effect of Nickel content and cooling rate on the microstructure of as cast 316 stainless steels. *Crystals* **2025**, *15*, 168. [CrossRef]
10. Wang, S.; Yang, H.; Jiao, G.; Ren, M.; Li, X. ECG analog front end circuit-A review. *Measurement* **2026**, *267*, 120566. [CrossRef]
11. Anami, K.; Sause, R.; Abbas, H.H. Fatigue of web-flange weld of corrugated web girders: 1. influence of web corrugation geometry and flange geometry on web-flange weld toe stresses. *Int. J. Fatigue* **2005**, *27*, 373–381. [CrossRef]
12. Wu, X.; Ouyang, X.; Tian, J.; Zheng, Y.; Yuan, J.; Wang, W.-W.; Zuo, Y.; Fu, H.; Yu, W.; Wang, R. Self-sensing mechanism and theoretical model of prestressed FRP-ECC multifunctional composite beams under bending loads. *Structures* **2026**, *87*, 111585. [CrossRef]
13. Hu, L.; Jia, P.; Wang, Z.; Wang, Y. Study on type of magnetic suspension rotor groove and wear of drop touchdown bearing. *Eng. Appl. Comput. Fluid Mech.* **2024**, *10*, 2422065. [CrossRef]
14. Fan, Y.; Yang, J.; Gao, S.; Liu, J.; Ma, T. Experimental study on the evolution of electro-erosion waves in bearing rollers under current-carrying conditions. *Sci. China Technol. Sci.* **2026**, *69*, 1820302. [CrossRef]
15. Lou, Z.; Song, C.; Ren, Y.; Pang, X.; Lu, H.; Du, S.; Zhang, Y. Formation of corrugated damage on bearing race under different AC shaft voltages. *Materials* **2024**, *17*, 859. [CrossRef] [PubMed]
16. Garnham, J.E.; Brightling, J.R.; Beynon, J.H. Rolling-sliding dry wear testing—A vibration analysis. *Wear* **1988**, *124*, 45–63. [CrossRef]
17. Pan, W.; Chen, Y.; Han, C.; Wang, J.; Bao, J. Rolling bearing fault vibration characteristic analysis software system accounting waviness and local defects. *Int. J. Reliab. Saf.* **2026**, *20*, 282–309. [CrossRef]

18. Harder, A.; Zaiat, A.; Becker-Dombrowsky, F.M.; Puchtler, S.; Kirchner, E. Investigation of the voltage-induced damage progression on the raceway surfaces of thrust ball bearings. *Machines* **2022**, *10*, 832. [CrossRef]
19. Song, C.; Ren, Y.; Huang, Q.; Zhang, Y.; Li, Y.; Cheng, J.; Pang, X.; Zhang, Y. Effect of shaft voltage on electric damage of GCr15 bearing material. *Tribol. Int.* **2024**, *200*, 110139. [CrossRef]
20. Zhou, R.; Li, M.; Liu, H.; Pan, W.; Zhang, R.; Liu, Y. Theoretical and experimental study on the evolution of contact load during wear failure of cylindrical roller bearings. *Eng. Fail. Anal.* **2025**, *169*, 109218. [CrossRef]
21. Graf, S.; Koch, O. Changes in surface topography and light load hardness in thrust bearings as a reason of tribo-electric loads. *Lubricants* **2024**, *12*, 303. [CrossRef]
22. Tauviqirrahman, M.; Jamari, J.; Setiyana, B.; Muchammad, M.; Prabowo, D. Performance analysis of a new design concept of journal bearing with surface roughness. *J. Tribol.* **2023**, *38*, 1–18.
23. Narwat, K.; Kumar, V.; Singh, S.J.; Kumar, A. Performance analysis of circular and lemon bore hydrodynamic journal bearing considering surface roughness and shear thinning effect. In *Aerospace and Associated Technology*; Routledge: London, UK, 2022; pp. 101–105. [CrossRef]
24. Litwin, W. Influence of surface roughness topography on properties of water-lubricated polymer bearings: Experimental research. *Tribol. Trans.* **2011**, *54*, 351–361. [CrossRef]
25. Yunlong, W.; Wenzhong, W.; Shengguang, Z.; Ziqiang, Z. Effects of raceway surface roughness in an angular contact ball bearing. *Mech. Mach. Theory* **2018**, *121*, 198–212. [CrossRef]
26. Li, X.; Wang, Y.; Pu, G.; Wang, K. Research on the Wheel Wear and Rolling Contact Fatigue of Metro Vehicle Induced by Rail Corrugation. *Tribol. Trans.* **2024**, *67*, 1168–1179. [CrossRef]
27. Liu, X.Y.; Yin, M.; Liu, C.Y.; Sun, J.; Shi, X.; Geng, L.; Yin, M. Effect of rolling surface texture on bearing friction pairs lubrication. *iScience* **2026**, *29*, 116521. [CrossRef] [PubMed]
28. Yue, L.; Liu, C.; Xin, Q.; Xu, W.; Wang, B.; Bai, P. Effect of temperature on the friction performance and mechanisms of Si3N4 and steel interfaces in oil-lubricated term rolling bearing. *Ind. Lubr. Tribol.* **2025**, *77*, 1360–1369. [CrossRef]
29. Hu, L.; Li, B.; Wang, Z.; Wang, Y. Analysis and evaluation of multi-state wear mechanism of elastic-flexible thin-walled bearings. *Tribol. Int.* **2025**, *202*, 110293. [CrossRef]
30. Hu, L.; Li, W.; Li, B.; Cui, B.; Wang, Z.; Wang, Y. Wear characteristics and mechanism evaluation of high-speed petal magnetic rotor series bearings (HPMRSBs) in vacuum. *Compos. Part B Eng.* **2025**, *313*, 113369. [CrossRef]
31. Hu, L.; Wang, Z.; Wang, J.; Wang, Y. Derivative Analysis and Evaluation of Roll-slip Fretting Wear Mechanism of Ultra-thin-walled Bearings under High Service. *Wear* **2024**, *562–563*, 205630. [CrossRef]
32. Hu, L.; Pueh, L.H.; Wang, Z.; Wang, Y. Surface performance control and evaluation of precision bearing raceway with wireless sensing CBN grinding wheel. *Wear* **2025**, *568*, 205966. [CrossRef]
33. Yin, C.; Dong, Y.; He, J.; Wang, Y. A fault evolution knowledge-driven adversarial meta-learning method for few-shot tool state recognition under variable working conditions. *Eng. Appl. Artif. Intell.* **2026**, *167*, 113806. [CrossRef]
34. Yin, C.; Sun, T.; Wu, H.; Dong, Y. Trustworthy multistep-ahead remaining useful life prediction for rolling bearings with limited data. *Reliab. Eng. Syst. Saf.* **2025**, *267*, 111902. [CrossRef]
35. Huang, S.; Liu, Z.; Yin, Y.; Liu, C. Generalizing Resistive Force Theory: Revealing and Modeling Nonlinear Intrusion Resistance in Solid-like Granular Matter. *J. Mech. Phys. Solids* **2026**, *216*, 106765. [CrossRef]
36. Wang, Y.; Huang, Q.; Xu, Z.; Wei, Z.; Zhang, X.; Zhang, Y.; Liu, W.; Qi, J. The investigation of flocculation and deposition of heavy components in the crude oil tank based on experiment and molecular simulation. *Fuel* **2023**, *353*, 129217. [CrossRef]
37. Chen, L.; Li, S.-Y.; Zhu, S.-Y.; Wang, T.; Huang, Q.-X. Physicochemical co-evolution of SUS304 ultra-thin steel foils induced by laser and its effect on interface bonding of steel/CFRP joints. *J. Iron Steel Res. Int.* **2026**, *32*, 80. [CrossRef]
38. Liu, M.; Tian, J.; Zhao, J.; Sun, Y.; Liang, J.; Zheng, Y.; Zhang, W.; Wu, X.; Yuan, J.; Fu, H. Seismic performance of CFRP-strengthened steel fiber reinforced concrete composite columns: Experimental, numerical and theoretical analyses. *Constr. Build. Mater.* **2025**, *505*, 144692. [CrossRef]
39. Tian, J.; Li, G.; Wu, X.; Yu, W.; Zuo, Y.; Yuan, J.; Wang, W.-W.; Fu, H.; Liu, M.; Wang, R. Self-sensing performance and theoretical model for the interface of self-sensing engineered cementitious composites and conductive concrete under shear loading. *Case Stud. Constr. Mater.* **2025**, *23*, e05618. [CrossRef]
40. Yin, C.; Li, Y.; Wang, Y.; Dong, Y. Physics-guided degradation trajectory modeling for remaining useful life prediction of rolling bearings. *Mech. Syst. Signal Process.* **2025**, *224*, 112192. [CrossRef]
41. Hu, L.; Ye, J.; Wang, Z.; Wang, Y. Evaluation of Active Magnetic Bearing System (AMB-S) and Touchdown Bearings (TDBs) Failure and Wear. *Results Eng.* **2026**, *32*, 113523. [CrossRef]
42. He, H.; Wang, P.; Li, X.; Zhang, Y.; Zhang, X. Highly reliable RS-PUF based on reconfigurable gas sensor array. *IEEE Sens. J.* **2024**, *24*, 16875–16882. [CrossRef]
43. Yan, J.; Chen, B.; Zhang, F.; Cheng, Y.; Wang, H.; Wang, H.; Wang, M.; Li, T.; Zhang, W. Meta-learning-based graph convolutional wavelet network for intelligent dynamic modeling of high-speed rail subsystems. *IEEE Trans. Veh. Technol.* **2026**, 1–16. [CrossRef]

44. Nan, Y.; Yu, J.; Li, X.; Wang, P.; Zheng, Y.; Wang, S. Temperature Compensation Method for Gas Sensors Based on Lightweight Mixture of Experts (MoE). *IEEE Sens. J.* **2025**, *21*, 25. [CrossRef]
45. Xue, Z.; Yang, K.; Li, Y.; Pei, C.; Hou, D.; Zhao, Q.; Wang, Y.; Chen, L.; Chen, C.; Mu, W. The Influence of Heat Treatment Process on the Residual Ferrite in 304L Austenitic Stainless Steel Continuous Casting Slab. *Materials* **2025**, *18*, 3724. [CrossRef] [PubMed]
46. Han, X.; Wang, S.; Yu, J.; Wang, P.; Li, X. Design of PUF based on a Cr2O3-SnO2 gas sensor for Internet of Things security. *Measurement* **2026**, *276*, 121395. [CrossRef]
47. Ni, L.; Huang, X.; Chen, X.; Pu, J.; Wang, A.; Xin, S.; Meng, Y. In-memory unified TRNG and PUF based on RRAM random switching time. *IEEE Trans. Electron Devices* **2025**, *72*, 6729–6739. [CrossRef]
48. Šafář, M.; Dütsch, L.; Harničárová, M.; Valíček, J.; Kušnerová, M.; Tozan, H.; Kopal, I.; Falta, K.; Borzan, C.; Palková, Z. Comprehensive prediction model for analysis of rolling bearing ring waviness. *J. Manuf. Mater. Process.* **2025**, *9*, 220. [CrossRef]
49. Tabaszewski, M.; Firlik, B. Detection of the presence of rail corrugation using convolutional neural network. *Eng. Trans.* **2022**, *70*, 339–353. [CrossRef]
50. Li, D.; Ye, J.; Chen, G.; Hu, L.; Wang, Z.; Qian, T. Performance evaluation of a halbach permanent magnet axial protection bearing under vertical magnetic levitation flywheel rotor drop. *Lubricants* **2026**, *14*, 40. [CrossRef]
51. Demas, N.G.; Lorenzo-Martin, C.; Luna, R.; Erck, R.A.; Greco, A.C. The effect of current and lambda on white-etch-crack failures. *Tribol. Int.* **2023**, *189*, 108951. [CrossRef]
52. Li, C.; Liu, P.Y.; Zhao, M.M.; Zhang, Y.F.; Bao, H.F.; Yang, M.; Chen, Y.Z.; Zhong, G.M. Regulation mechanism of dielectric constant onion transport behavior in vinylidene fluoride-based solid composite electrolytes. *Electrochim. Acta* **2026**, *573*, 149499. [CrossRef]
53. Xue, Z.; Hou, D.; Chen, L.; Su, Z.; Liang, J.; Ma, S.; Li, Z.; Yang, K.; Sun, Y.; Chen, C. Effect of Nickel Content and Cooling Rate on the Microstructure of As-Cast 316 Stainless Steels Part II: Ferrite and Precipitated Phases Under the Same Sampling Conditions. *Crystals* **2026**, *16*, 508. [CrossRef]
54. Liu, E.; Wang, X.; Li, J.; Chen, C.; Li, Q.; Lv, X.; Dang, J. Two-dimensional lamellar TiO2 surface-loaded RuCo nanoclusters for pH-universal electrocatalytic hydrogen evolution. *J. Mater. Sci. Technol.* **2026**, *254*, 71–80. [CrossRef]
55. Guo, J.N.; Chen, C.; Dong, X.R.; Li, X.L.; Zhao, Q.H.; Zhang, M.X.; Yang, C.G. Multi-functional liquid metal/carbon nanotubes/bacterial cellulose flexible composite film, suitable for electromagnetic shielding, intelligent wearable sensors and joule heater materials. *Olloids Surf. A-Physicochem. Eng. Asp.* **2026**, *752*, 141829. [CrossRef]
56. Guo, J.N.; Dong, X.R.; Ji, X.D.; Li, X.L.; Zhao, Q.H.; Zhang, M.X.; Yang, C.G. High-strength and flexible cross-linked Poly (vinyl alcohol-co-ethylene)/UHMWPE/Fe_3O_4@RGO nanofiber film for high-performance electromagnetic shielding. *Surf. Interfaces* **2026**, *100*, 110979. [CrossRef]

Disclaimer/Publisher's Note: The statements, opinions and data contained in all publications are solely those of the individual author(s) and contributor(s) and not of MDPI and/or the editor(s). MDPI and/or the editor(s) disclaim responsibility for any injury to people or property resulting from any ideas, methods, instructions or products referred to in the content.